ADVANCED MATERIALS TECHNOLOGIES
www.advmattechnol.de

Dual-Material Aerosol Jet Printing of Magneto-Responsive Polymers with In-Process Tailorable Composition for Small-Scale Soft Robotics

Silvia Taccola, Hadi Bakhshi, Midori Sanchez Sifuentes, Peter Lloyd, Luke J. Tinsley, James Macdonald, Alistair Bacchetti, Oscar Cespedes, James H. Chandler, Pietro Valdastri, Wolfdietrich Meyer, and Russell A. Harris**

The opportunity to create magneto-responsive soft materials (MSMs) with in-process tailorable and locally controllable magnetic properties is highly desirable across many technological and biomedical applications. In this paper, this capability is demonstrated for the first time using computer-controlled dual-material aerosol jet printing (DMAJP) technology. This approach allows controlled variation of composition between the aerosols of a magnetic nanoparticles (MNPs) ink and a photocurable polymer during the printing process. The mixing ratio of the two aerosols determines the MNPs loading in the nanocomposite, which can be used to locally control the magnetic properties of the printed structures. The printing process is structured in a layer-by-layer fashion in combination with a sacrificial layer approach for building fully freestanding MSM structures that combine magnetoactive and non-magnetoactive elements in a single process multi-material printing method with no further assembly requirements. Using this method, the direct manufacturing of small-scale multi-material soft objects with complex shapes and programmable functions whose movements can be controlled by the application of an external magnetic field is demonstrated.

1. Introduction

Inspired by the amazing examples of responsive actuation seen in biological systems, a new generation of researchers across the world is investigating soft composite materials that respond to changes in their environment and provide stimuli-triggered deformation while being efficient and sustainable.[1] These materials provide unique advantages including mechanical compliance, lightweight, low cost, and flexible processing. The ability to reversibly shape-change in response to a given stimulus, such as heat, electrical and/or magnetic fields, light, or chemical changes, has high-value applications across many fields, including soft robotics, drug delivery, and biomedical devices.[2]

Amongst stimuli-responsive materials, magneto-responsive soft materials (MSMs) consist of magnetic particles (e.g., ferrites, magnetite, neodymium particles) embedded in a soft polymeric matrix (e.g., elastomers, hydrogels). In particular, the use of ferromagnetic materials, which have a strong response to an externally applied magnetic field, has led to the development of magnetically actuated and controlled soft robots.[3] These provide functions such as; remote wireless control, miniaturization potential, fast response speed, and harmless interaction with tissues.[3,4] As a result, MSMs are excellent candidates for the next generation of untethered soft robots, biomimicking structures, and soft manipulators, with a particular benefit for medical applications.[5]

Control over the spatial distribution of the magnetic particles embedded in the polymer matrix is critical and often challenging. MSMs that combine magneto-active and non-magnetic elements exhibit a spatially anisotropic response to the applied magnetic field and have demonstrated enhanced controllability and manipulation efficiency compared with structures solely made of magneto-active materials.[5c,6] Within this framework, a key challenge is the availability of effective and efficient manufacturing processes to implement complex multiple-material patterning and integration at an appropriate scale. MSMs with locally controlled composition can be made by preparing the

S. Taccola, M. Sanchez Sifuentes, L. J. Tinsley, J. Macdonald, R. A. Harris
Future Manufacturing Processes Research Group
University of Leeds
Woodhouse, Leeds LS2 9JT, UK
E-mail: s.taccola@leeds.ac.uk; r.harris@leeds.ac.uk
H. Bakhshi, W. Meyer
Fraunhofer Institute for Applied Polymer Research IAP
Geiselbergstraße 69, 14476 Potsdam, Germany
P. Lloyd, A. Bacchetti, J. H. Chandler, P. Valdastri
STORM Lab
University of Leeds
Woodhouse, Leeds LS2 9JT, UK
O. Cespedes
School of Physics and Astronomy
University of Leeds
Woodhouse, Leeds LS2 9JT, UK

The ORCID identification number(s) for the author(s) of this article can be found under https://doi.org/10.1002/admt.202400463

DOI: 10.1002/admt.202400463

magnetic and non-magnetic segments separately using conventional manufacturing processes, such as casting/molding, and assembling the final structure by the use of manual or template-assisted processes.[5c,6c,7] This reduces the efficiency and flexibility of the overall fabrication process and hence limits both its reproducibility and scalability for high-volume fabrication. Significantly, these approaches are also limited in both the complexity and resolution of the devices that can be created, with the consequential constraints on their functionality. Recently, emerging multi-material additive manufacturing (MMAM) technologies have captured attention as an alternative to template-based processes to eliminate complex and time-consuming assembly, whilst introducing rapid and flexible design-manufacturing cycles, less material waste, and opportunities for device personalization.[8] MMAM technologies have been successfully employed for the easy and rapid fabrication of devices with a wide range of properties and functionalities (e.g., mechanical, optical, chemical, and electrical).[9] However, the development of MMAM technologies that enable the automatic fabrication of small-sized multi-material MSM objects with complex geometries is particularly challenging due to the unconventional materials used in this field (i.e., soft polymers and magnetic particles). Within this framework, the use of Poly Jet printing is severely limited by its restriction to low viscosity inks, which significantly limits the range of soft polymers processable by this technology, and by nozzle clogging issues due to aggregation and sedimentation of magnetic nanoparticles (MNPs).[10] As an alternative to polyjet printing, different MMAM methods have been proposed, including direct ink writing (DIW),[11] digital light processing (DLP),[6a] and magnetic field-assisted projection stereolithography (M-PSL).[6b,12] However, DIW has the limitation of relatively low resolution, while stereolithography-based processes generally have poor multi-material capabilities.[13] To date, the availability of an effective, efficient, flexible, and sustainable manufacturing process that allows the creation of combined non-magnetic and magnetic materials with a wide variety of material options and high manufacturing resolution still remains a major challenge.[14]

This research demonstrates the use of Aerosol Jet Printing (AJP) as an enabling manufacturing process that could facilitate the next generation of MSMs. AJP is a contactless direct write approach with distinct advantages in terms of fast prototyping, wide ink compatibility, and a maximum printing resolution of the order of 10 μm.[15] AJP enables the use of inks with much higher viscosity (up to 1000 cp) and larger particle sizes and loadings compared to inkjet-based printing,[16] two particularly appealing features for the fabrication of MSMs. Moreover, although AJP has primarily been used for surface patterning and the printing of 2D structures, researchers are beginning to explore its potential for producing truly 3D microstructures with complex architectures.[17] Such capability further supports the potential value of AJP in the MSM field. In a typical AJP process, ink is first pneumatically or ultrasonically atomized into aerosol droplets and then transported to the deposition head using a carrier gas flow. Here the aerosol is collimated and accelerated by a further annular sheath gas and then focused through a nozzle. AJP can be modified and used in a dual-material configuration (DMAJP) in which two different inks are simultaneously used in the printing process from separate atomizers and the resulting aerosols are mixed in situ in the aerosol flow path prior to deposition through a single nozzle (**Figure 1a**).[18] By tuning the two ink flow rates, it is possible to adjust the mixing ratio on-demand between the two ink aerosols during the AJP process, which can be used to locally control the composition of the printed nanocomposite while achieving high-resolution material patterning. This in-process control of the composition is a significant feature that cannot be achieved in conventional multi-material printing using feedstocks in liquid/liquid or liquid/solid phases.[18b] Moreover, since two different materials are held and atomized in two separate ink containers and only the aerosols generated from the atomization process are mixed, DMAJP can overcome difficulties associated with mixing incompatible inks, making possible the mixing of two different dispersions or solvent media (e.g., mixing of water-based ink and oil-based ink).[19] The use of DMAJP for nanocomposite manufacturing is still very novel and few articles exist in the literature, mainly focusing on the deposition of conductive nanocomposites with variable electrical properties.[18a,19a,20] In the field of magnetic materials, Craton et al. recently reported the use of DMAJP for the deposition of nickel-zinc ferrite nanoparticles/polyimide nanocomposites for microwave packaging applications.[21]

In other published work, Taccola et al. demonstrated the use of AJP to reliably produce micro-scale patterns of MNPs on existing structures of soft and flexible polymers commonly used in soft robotics and biomedical engineering applications.[22] In this present work, the use of DMAJP to combine and shape polymeric and magnetic materials into various multi-material objects in a single manufacturing process is investigated. In-house developed magnetic ink and photopolymer ink were selected to investigate DMAJP for the fabrication of free-standing and self-supported MSMs with in-process tailorable and controllable composition. The process involves the stack-printing of layers of different materials with the desired magnetic functionality onto a substrate coated with a water-soluble sacrificial film that is subsequently dissolved to release the freestanding structure. As a proof-of-concept, a set of magnetically responsive soft objects with complex shapes and programmable functions whose movements can be controlled by the application of an external magnetic field has been created. This versatile and controllable multi-material fabrication method has the potential to greatly extend the capability of 3D printing for applications featuring remote magnetic control, such as for biological, medical, and robotic fields.

2. Results and Discussion

2.1. Formulation of the Magnetic and Polymer Ink

An important stage in the proposed DMAJP process is the formulation of two inks, namely magnetic and polymer ink, with physical properties such as viscosity and particle dimensions suitable for aerosolization. The Optomec Aerosol Jet print engine used in this work has two separate atomization options: the ultrasonic atomizer (UA), which produces aerosol from low-viscosity inks (1–10 cp), and the pneumatic atomizer (PA), which enables the atomization of materials with a viscosity up to 1000 cp.[15] Starting from previous knowledge in aerosol jet printing of magnetic materials, a customized magnetic ink specifically

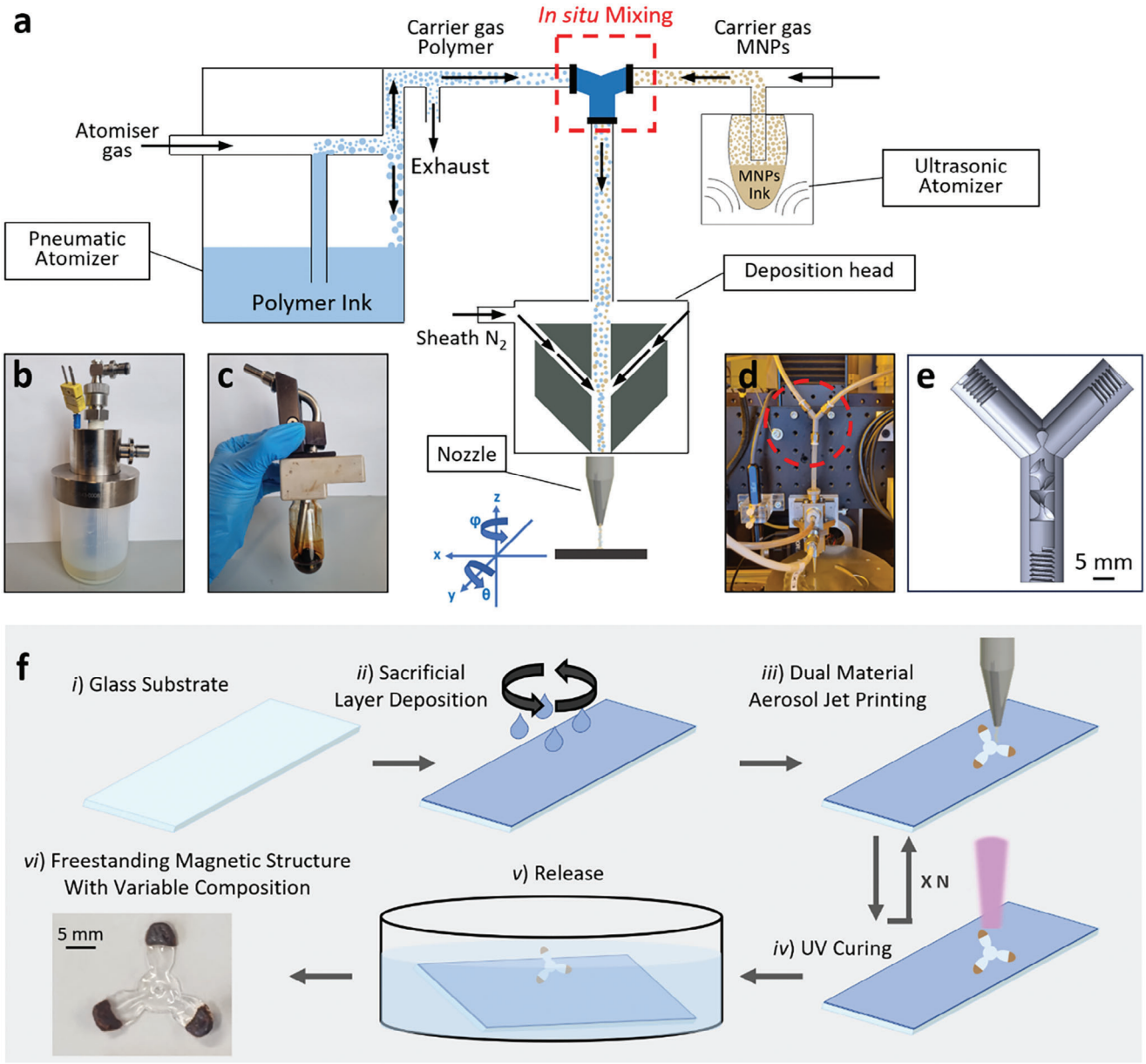

Figure 1. a) Schematic illustration of the DMAJP process. b) Polymer ink in the plastic jar for pneumatic atomization. c) Magnetic ink in the glass vial for ultrasonic atomization. d) and e) The static mixing chamber used for the in situ mixing of the two aerosols. f) Overview of the fabrication process for the creation of freestanding magnetic soft composite structures: (*i*) and (*ii*) deposition of a water-soluble sacrificial layer of polyvinyl alcohol (PVA) on top of a glass substrate by spin-coating; (*iii*) and (*iv*) cyclic alternated DMAJP deposition and UV curing of the printed pattern in a multi-layered fashion; (*v*) and (*vi*) dissolution of the sacrificial layer by immersion of the sample in a petri-dish filled with deionized water and the subsequent release.

formulated and optimized for ultrasonic AJP deposition was used in the present work.[22] For the formulation of this ink, Fe_3O_4 nanoparticles of 10 nm diameter were selected in light of their size being compatible with ultrasonic atomization (<50 nm) (see Experimental section for details). Regarding the polymer ink, the key criteria used for the selection are: 1) a viscosity <1000 cp for the PA atomization process, 2) a low Young's modulus of the cured material, which allows high mechanical compliance and deformability to be suitable for soft robotic applications, and 3) biocompatibility desirable for biomedical applications. Our choice was directed to in-house manufactured urethane-acrylate-based photo-curable inks recently developed for 3D printing applications and previously tested on a digital light processing machine.[23] While the majority of photo-curable inks are cytotoxic due to the unreacted monomers, photoinitiator residuals, and toxic impurities, the selected materials are synthesized via a safe and environmentally friendly route in the absence of toxic isocyanates and tin compounds, making them excellent candidates for biomedical applications.[23b] Moreover, their mechanical properties can be tailored to the specific application depending on the formulation.[23a] For this work, a photopolymer ink formulation with a viscosity compatible with pneumatic

atomization (48 cP) and an elastic modulus of the photo-cured bulk material of 17 MPa has been selected (see Experimental section for details).[23a] Prior to multi-material printing experiments, the capability of processing the selected photopolymer ink by AJP was first demonstrated in a single material configuration using the pneumatic atomization mode, and the results are reported in Section S1 (Supporting Information).

2.2. Fabrication of magnetic soft materials by DMAJP

A schematic illustration of the developed DMAJP process is reported in Figure 1a (see also Experimental Section). To fabricate magneto-responsive nanocomposite polymers, the photopolymer ink was placed in the plastic jar for pneumatic atomization (Figure 1b) while the magnetic ink was placed in the glass vial for ultrasonic atomization (Figure 1c). A static mixer allows in situ mixing of the ink aerosols generated from the two different atomization methods just prior to deposition (Figure 1d,e). The static mixer was added to achieve a homogeneous mixing of the two aerosols, as described in more detail in Section S2 (Supporting Information).

The different steps of the developed fabrication procedure are shown in Figure 1f (see also Experimental section). A mask- and assembly-free, time- and material-saving approach based on DMAJP and structured in a layer-by-layer fashion in combination with a sacrificial layer approach is proposed, which allows to fabrication of fully printed self-supported freestanding MSMs-based objects with different shapes and magnetic composition. The properties of DMAJP printed composites are determined by the configuration and the interplay of printing process parameters, such as aerosol ink carrier flow rates, sheath gas flow rate, printing speed, etc.[18b] In this study, a default configuration setting was defined for the printing of the photopolymer (see Experimental Section and Section S1, Supporting Information for details). Once these parameters were fixed, the carrier gas flow rate of the MNPs aerosol was varied to control the MNPs loading in the printed nanocomposite film. MNPs loading is controlled by the ratio of MNPs aerosol to the polymer aerosol, denoted as mixing ratio r (Equation 1).

$$r = \frac{Carrier\ gas\ flow\ rate\ MNPs}{Carrier\ gas\ flow\ rate\ polymer} \quad (1)$$

Since MNPs compete with the photoinitiator in absorbing the incident radiation, inhibiting radical formation, and affecting the photopolymerization process, there is a limitation in the amount of MNPs that can be added to any photocurable polymer.[24] In the present work, the carrier gas flow rate of the MNPs aerosol was gradually increased until the photopolymerization was hindered and a wet, sticky film was obtained, allowing to identification of the maximum r to preserve a satisfactory degree of photopolymerization (Section S3, Supporting Information). Notably, the deposition of the composite in a multilayer fashion, by cyclic alternating DMAJP deposition and UV curing of subsequent thin layers of materials, has a beneficial role in maximizing the content of MNPs in the composite. Previous studies have indeed demonstrated that high contents of magnetic particles can be achieved only at the cost of drastically decreasing the composite film thickness.[24c]

2.3. Morphological Characterization

For morphological characterization, the content and distribution of MNPs in the polymer matrix were tested on thin film rectangular samples with 20 mm length and 5 mm width (see Figure S1d, Supporting Information). The samples were referred to as MNP-CF_x denoting MSMs prepared using x carrier gas flow rate of the MNPs aerosol (x = 0, 50, 60, 70, 80 SCCM) with r 0.1, 0.12, 0.14, and 0.16, respectively. The quality of the obtained printed nanocomposite was initially checked by digital optical microscopy on 1-layer samples supported over the fabrication substrate. Representative optical microscopy images are reported in **Figure 2**a–d. No samples showed holes, cracks, or other discontinuities caused by inadequate printing process parameters, inefficient solvent evaporation, or a low wettability of the printing substrate. All samples showed the presence of clusters of MNPs in the transparent polymer matrix, with the number of clusters and their aggregation increasing as the flow rates of the MNPs aerosol increase. However, a quite constant dispersion is maintained even when higher MNPs loadings are reached (MNP-CF_{80}, Figure 2d). The clustering phenomenon is influenced by several factors. Cluster formation can be due to the low miscibility of the toluene (i.e., the main solvent of the magnetic ink) with the photopolymer ink. Even if the mixing in the aerosol form rather than in liquid form makes it possible to mix two incompatible inks,[19] the use of solvent media with poor miscibility leads to a certain degree of particle aggregation. Moreover, the higher MNPs loadings in higher MNPs flow rate samples reduce the mean interparticle distance during the curing and evaporative phase of the deposition process, causing aggregation by attractive van der Waals forces between the particles.[25] The possibility of aggregation driven by magnetic interaction can be excluded: as will be shown by superconducting quantum interference measurement device (SQUID) analysis, the absence of remanence or coercivity in the magnetization hysteresis loops of all samples confirmed that the MNPs have no magnetic attraction for each other.[26] The clustering phenomenon could be improved by treating the particles with other solvents or surfactants with better miscibility with the polymer. However, the presence of MNPs aggregates does not affect the proposed application, as will be demonstrated in the following paragraphs.

Surface analysis using a scanning electron microscope (SEM) and energy dispersive X-ray (EDX) were performed to deeply investigate the particle dispersion in the nanocomposite (see Experimental section for details). SEM (Figure 2e–h) and EDX (Figure 2i-l) observations confirmed an increasing amount of Fe_3O_4 nanoparticles in the films increasing the flow rate of the MNPs aerosol. The EDX spectrum analysis curve of pristine MNPs and the pure polymeric sample, used as a comparison, are reported in Section S4 (Supporting information).

Because the nanocomposite films are printed layer by layer, the printing of multiple layers allows for control of the thickness of the printed patterns. The dependence of the thickness on the number of layers has been investigated by optical profilometer measurements, and the results are reported in Figure 2m. Measured were performed for MNP-CF_0 and MNP-CF_{80}. As expected, for each flow rate of the MNPs, the thickness linearly grows by increasing the number of layers, with a layer-by-layer growth rate of 18 ± 0.5 µm and 15 ± 0.2, respectively for MNP-CF_0 and

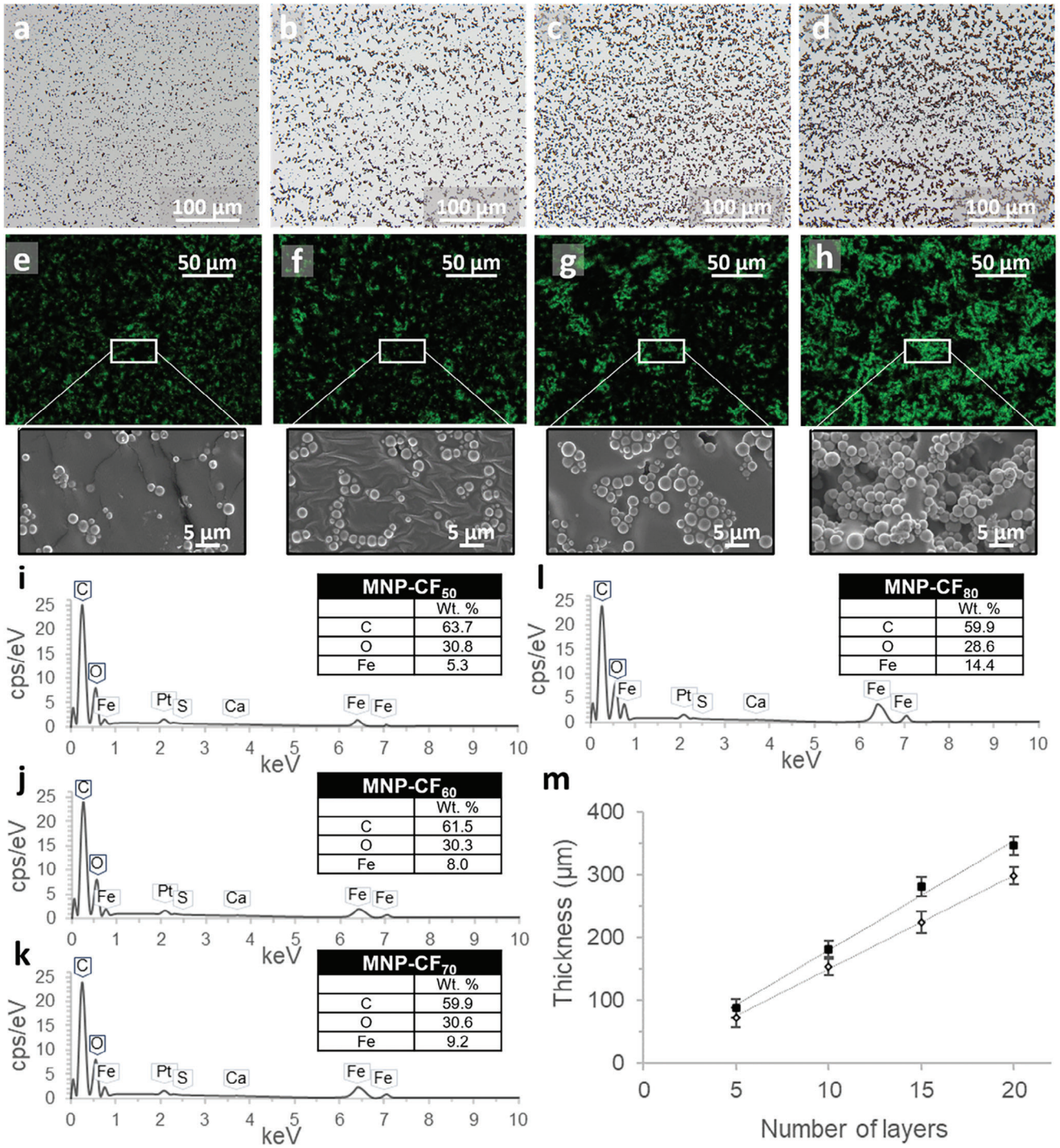

Figure 2. Optical microscope, scanning electron microscope micrographs at different magnification values and energy dispersive X-ray (EDX) analysis of MNP-CF_x samples illustrating the trend of the changes in MNPs content by increasing the MNPs carrier gas flow rates: a), e) and i) MNP-CF_{50}, b), f) and j) MNP-CF_{60}, c), g) and k) MNP-CF_{70}, d), h) and l) MNP-CF_{80}. j) The dependence of the thickness on the number of layers for purely polymeric MNP-CF_0 sample (■) and composite MNP-CF_{80} samples (◊).

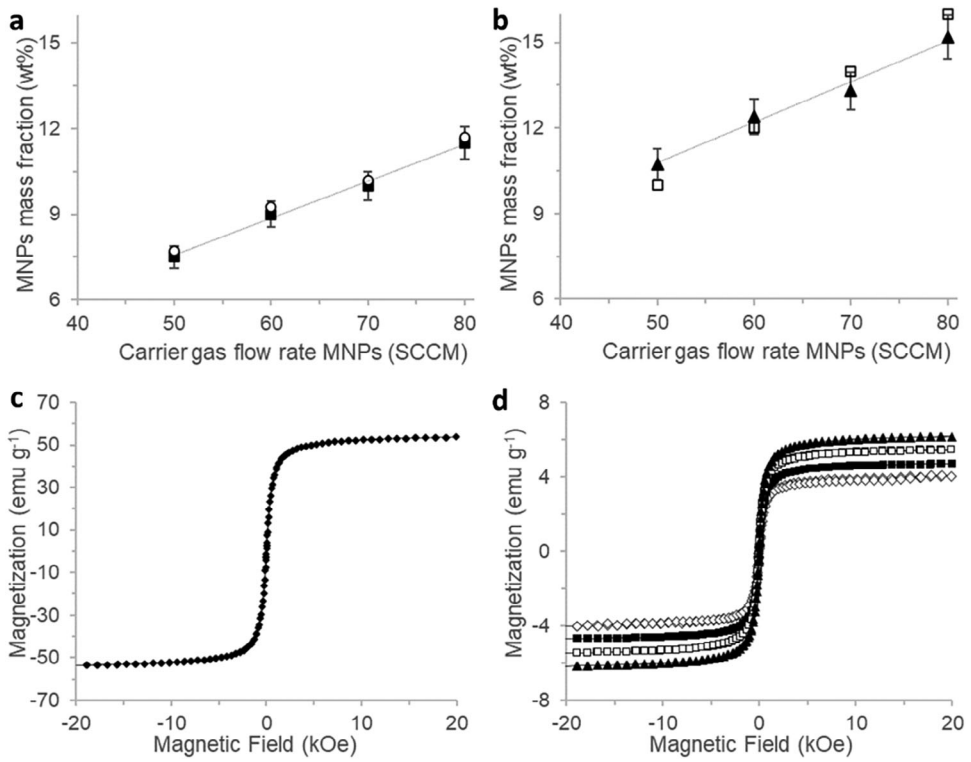

Figure 3. a) Mass fraction of MNPs estimated by TGA (■) and SQUID measurements (○) for different flow rates of the MNPs aerosol. b) Mass fraction of MNPs including their polymer coating estimated by TGA (▲) and relative mixing ratio *r* (□), expressed in percent. Magnetization hysteresis plots of c) pristine MNPs and d) DMAJP composite samples (◇) MNP-CF_{50}, (■) MNP-CF_{60}, (□) MNP-CF_{70} and (▲) MNP-CF_{80}.

MNP-CF_{80}. This demonstrated that the obtained film thickness depends on the amount of magnetic particles added, being typically slightly lower for films with higher MNPs contents, due to the lower degree of curing.[24b]

2.4. Thermogravimetric Analysis (TGA)

During the DMAJP process, the mass fraction of MNPs in the printed composite is not known as precisely as it would be if the composite was mixed before fabrication.[19a] Since the mixing ratio *r* is based on ink mist flows, the mass fraction of nanoparticles in the MNP-CF_x samples was measured after the printing by thermogravimetric analysis (TGA). The TGA results of the thermal degradation of the samples in the form of weight percent versus temperature are shown in Section S5 (Supporting information). The mass fraction of Fe_3O_4 MNPs in the composites (*w*) can be estimated from the remaining mass at the final temperature (600 °C) being the metal core of the pristine MNPs nonvolatile in this temperature range and the results are reported in **Figure 3**. As expected, a linear increase of MNPs content can be observed in the dependence of the flow rate of the MNPs aerosol, with a maximum of 11.5 wt% for MNP-CF_{80} (Figure 3a). It is important to note that the mass fraction measured by TGA refers to the Fe_3O_4 core of the pristine MNPs without considering their polymer coating, which also volatilizes together with the polymer matrix at 600 °C (see Section S5, Supporting information). From the thermogravimetric curve of the pristine MNPs, it is possible to estimate the mass fraction of MNPs including their polymer coating, resulting in 10.9, 12.4, 13.3, and 15.1 wt% for respectively MNP-CF_{50} MNP-CF_{60} MNP-CF_{70} and MNP-CF_{80}. It is noteworthy that these values are comparable to the mixing ratios *r* (i.e., 0.1, 0.12, 0.14, 0.16), implying that the polymeric and magnetic inks have similar atomization rates (Figure 3b).

2.5. Magnetic Properties of the Printed Samples

To characterize the magnetic response of the printed MNP-CF_x samples, their magnetization hysteresis was evaluated by a superconducting quantum interference measurement device (SQUID) and compared to the magnetization hysteresis of pristine MNPs. Hysteresis loops for pristine MNPs (Figure 3c) and composite samples (Figure 3d) showed no remanence or coercivity, thus indicating superparamagnetic behavior for all the samples, suggesting that the inclusion of the MNPs in the polymeric matrix by the DMAJP process did not significantly alter their magnetic properties. The superparamagnetic nature of the samples was confirmed through field-cooled and zero-field-cooled (FC-ZFC) protocols (see Section S6, Supporting information). Assuming that the magnetization of the composite films measured during the hysteresis loops is exclusively due to the metal core of the pristine MNPs present within them, their magnetic behavior can be described by superparamagnetic modeling, with the saturation magnetization depending only on the nanoparticle number density.[27] The magnetization evaluation can be used as an

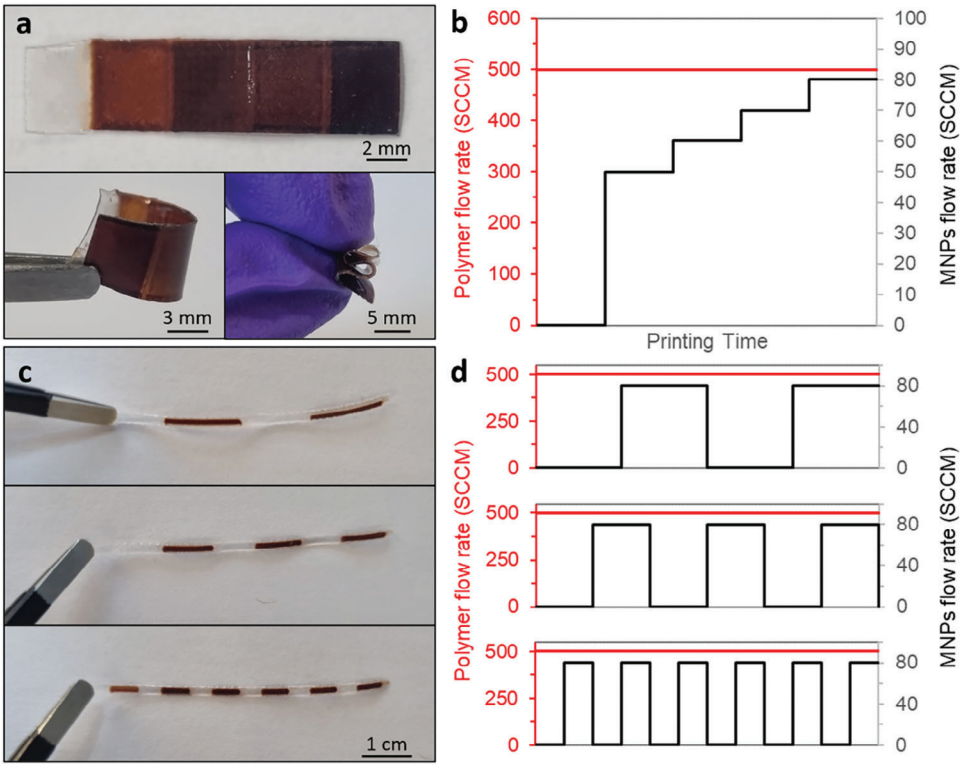

Figure 4. a) A printed nanocomposite film with five different MNPs content regions. From the left to the right, MNP-CF_0, MNP-CF_{50}, MNP-CF_{60}, MNP-CF_{70}, and MNP-CF_{80}. b) The flow rates of the polymer and MNP aerosol during the printing of 1 layer. c) Elongated printed structures combining magnetic and non-magnetic elements of different lengths and the corresponding flow rate profiles during the printing of 1 layer.

indirect measurement of the Fe_3O_4 MNPs mass fraction in the nanocomposite because they are the only magnetically active elements in the composite.[27,28] The MNPs mass fraction can be indirectly obtained from the ratio of the saturation magnetization per unit mass of the MNP-CF_x samples with that of the pristine powder. As displayed in Figure 3a, the concentrations of MNPs (without considering their polymer coating) previously obtained from the TGA results, are in good agreement with the magnetic measurements. The results confirmed that magnetization measurements can be useful for a good estimation of the MNPs mass fraction in the composite films, with the advantage that the measurements take less time and are non-destructive as compared to TGA investigations.[28]

2.6. Demonstration of the Ability to Tailor Material Composition During Printing

A unique characteristic of the proposed DMAJP method for the fabrication of MSMs is the possibility to control the MNPs loading at different regions of one nanocomposite film in situ during the printing. Different showcase examples were designed to demonstrate this capability and are reported in **Figure 4**. First, a 5 mm wide and 20 mm long nanocomposite film with 5 different MNPs loading regions of 4 mm width was printed and is shown in Figure 4a. The use of a soft and flexible polymeric matrix allows us to obtain composite structures that can be easily folded and deformed without breaking (see Figure 4a, bottom). The corresponding flow rates of the two aerosols during the printing are plotted in Figure 4b. Both the motion of the automated deposition stage and the DMAJP flow rates are controlled during the printing through the same machine control code (see Experimental section for details) allowing for easy control over the spatial distribution of the magnetic particles in the MSMs. In order to further demonstrate this, 1 mm wide, and 60 mm long strips composed of alternating magnetic and non-magnetic segments were printed, controlling and tuning the length of the segments (i.e., 1.5, 1, and 0.5 cm, Figure 4c). The corresponding flow rates of the two aerosols during the printing are plotted in Figure 4d. The individual strips shown in Figure 4c were printed within a period of ≈10 min, confirming the rapid and automated fabrication in a single printing process without the need for complicated and time-consuming assembly. These examples were selected to demonstrate that DMAJP can be easily used to combine polymeric and magnetic materials into multi-material objects in a single manufacturing process. In addition to this, the fabrication of more complex shapes and designs is illustrated in the next paragraph.

2.7. Proof-of-Concept Demonstrations

The following proof-of-concept demonstrators were created to show that the developed fabrication procedure can be used to combine and shape polymeric and magnetic materials into various small-scale multi-material soft objects whose movements can

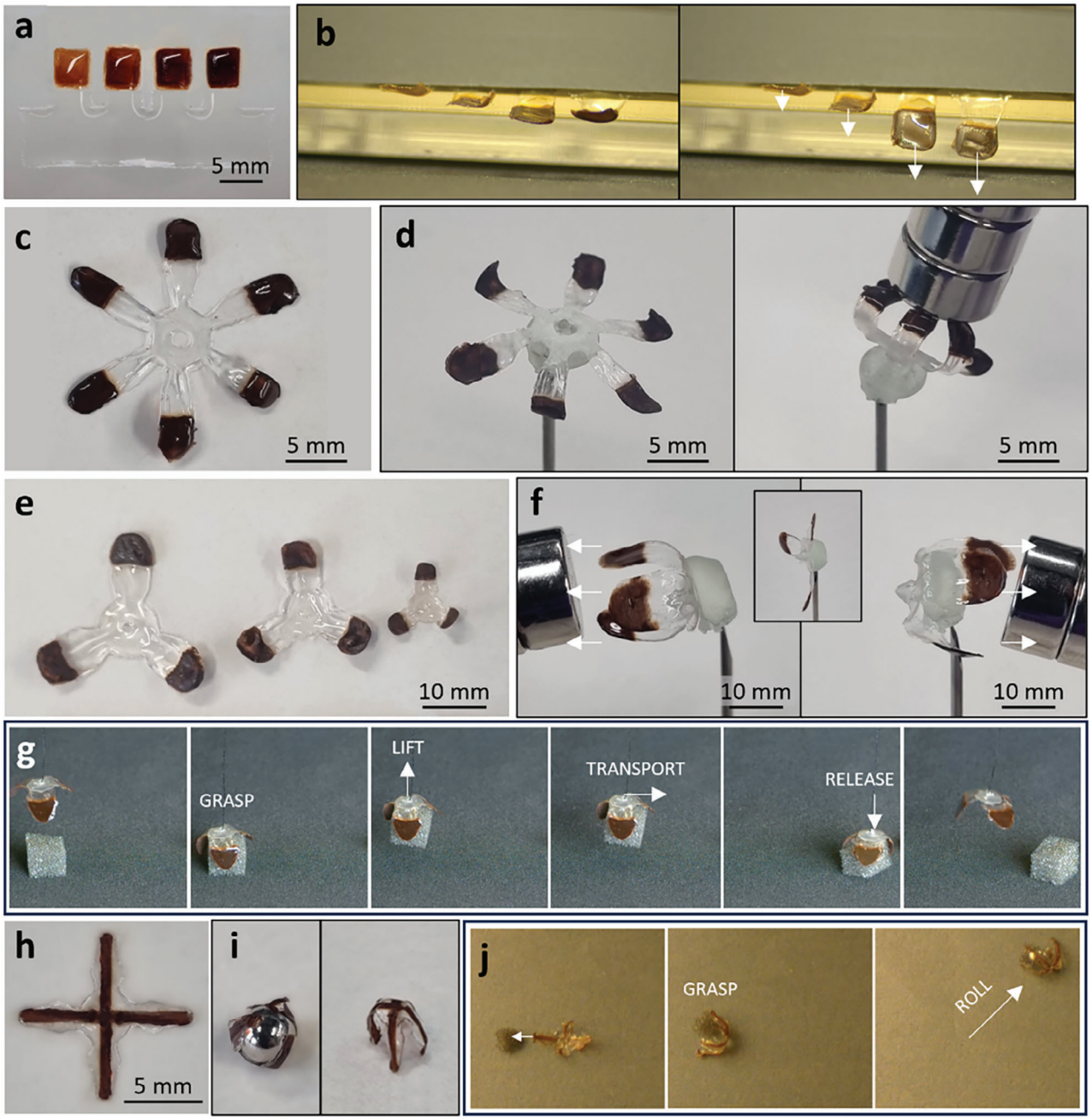

Figure 5. DMAJP printed MSMs-based multi-material soft objects with different design and motion capabilities: a) a 4-fingered soft object with increasing MNPs content in the fingertips (from the left to the right MNP-CF0, MNP-CF50, MNP-CF60, MNP-CF70, and MNP-CF80); b) the variable bending of the fingers when exposed to a magnetic field gradient; c) a flower-shaped object; d) bending motion of flower petals when exposed to a magnetic field gradient; e) 3-fingered grippers with different body diameter (from the left 20, 15, and 10 mm); f) bidirectional bending of the gripper when exposed to a magnetic field gradient from opposite side of its body (natural resting position in the inset); g) a gripper prototype used to demonstrate the ability to lift a lightweight, compressible object (a piece of polyurethane foam); h) the untethered rolling grasper in a planar configuration and in a folded configuration (i) after post-curing around a spherical magnet; j) untethered grasping and rolling movement of the grasper.

be controlled by applying an external magnetic field. In particular, different types of motion have been investigated, such as folding/unfolding, translation, and rolling.

First, a multi-material soft object composed of a purely polymeric main body (i.e., MNP-CF_0) and 4 beam-shaped fingers with a magnetic tip was fabricated (**Figure** 5a). The fingers are 4 mm wide, 8 mm long and have a 4 mm long magnetic tip with increasing MNPs content (from the left to the right MNP-CF_0, MNP-CF_{50}, MNP-CF_{60}, MNP-CF_{70}, and MNP-CF_{80}, Figure 5a). Thanks to the flexibility and softness of the photocurable polymer, typical features of materials for soft robotics, the fingers bend when exposed to the attractive force of a magnetic field

gradient (Figure 5b). It is noteworthy that the magnetic response of the fingers depends on the content of MNPs in the tip, with the bending amplitude increasing by increasing the MNPs content (Figure 5b; see also Section S7 and Video S1, Supporting Information). This demonstrated that the developed fabrication procedure enables structures with locally controllable magnetic responses to be produced in a single mask-free and assembly-free fabrication process.

In order to demonstrate the ability to easily change the design, a flower-shaped object, with a purely polymeric central body and six 7 mm-long petals with the highest content of MNPs in the magnetic tip (i.e., MNP-CF_{80}) to maximize the magnetic response, was fabricated (Figure 5c). As expected, the flower petals bend and close when exposed to the attractive force of a magnetic field gradient (Figure 5d). This folding/unfolding capability was leveraged to create the first proof-of-concept manipulator in the form of a 3-finger gripper. To demonstrate the dimensional scalability of the process, three grippers of different length scales were created (20-, 15- and 10-mm overall diameter, Figure 5e). As illustrated in Figure 5f, the grippers showed bidirectional bending capability when an external magnetic field gradient was applied from the opposite side of their body, allowing the fingers to bend in opposite directions. The ability of the grippers to grasp, lift, and deposit soft, highly compressible objects via the application of magnetic field gradient from below was demonstrated (Figure 5g, see also Section S8 and Video S2, Supporting Information).

Finally, an untethered rolling grasper was produced to demonstrate translation/rolling and folding/unfolding motions (Figure 5h). Compared to the earlier flower petals and grippers, this demonstrator exhibits a 3D referential position, being in a folded state at rest (Figure 5i, right). This was achieved by releasing the sample from the fabrication substrate before the final post-curing step (see Experimental Section), and then post-curing in a folded configuration around a spherical magnet (Figure 5i, left). This curved configuration allows the grasper to roll during translation as well as unfold/fold under the application of differing external magnetic field gradients (Figure 5j, see also Section S9 and Video S3, Supporting Information). Thanks to these behaviors the untethered grasping and locomotion of a compressible polyurethane foam ball were demonstrated via the manual application of a moving magnetic field gradient. The capability of the developed DMAJP printed objects to maintain a desired 3D referential position is a design tool currently under further investigation.

These preliminary proof-of-concept demonstrators confirmed the potential value of the proposed technique for fabricating small-scale magnetically controlled structures that can find application in the field of soft robotics. Of course, further research, design studies, and development will be required depending on the specific application.

3. Conclusion

This investigation provided a new straightforward mask- and assembly-free, versatile, time- and material-saving method based on computer-controlled DMAJP for the fabrication of MSMs with in-process tailorable composition. Two AJP printable inks were formulated, consisting of a customized Fe_3O_4 nanoparticle-based magnetic ink and an in-house developed soft and biocompatible photo-curable polymer ink. In situ, mixing of the two inks in the aerosol form prior to deposition allows the production of MSMs with locally controlled magnetic composition by in-process controlling the mixing ratio of the two aerosols. The adopted processing strategy is particularly appealing because it enables rapid and simple fabrication of small-scale multi-material objects combining magnetoactive and non-magnetic materials and locally controllable magnetic response with different designs in a single printing process. As a proof-of-concept, several MSM-based small-scale objects with different designs were printed to demonstrate various magnetically controlled movements, including translation, rolling, and folding/unfolding movements.

This study goes in the direction of extending the capability of 3D printing for the fabrication of magneto-responsive small-scale soft structures with a broad palette of advanced applications in the biological, medical, and robotic fields. Some elements requiring further research exist. First, the size limitation of MNPs for compatibility with ultrasonic atomization (diameter <50 nm) has oriented our initial choice toward the use of easily available superparamagnetic Fe_3O_4 nanoparticles. Despite Fe_3O_4 nanoparticles being highly relevant in many biological and biomedical applications due to their high biocompatibility, low toxicity, high magnetic susceptibility, and high saturation magnetization, their application for producing actuation is limited by the absence of magnetically hard behavior (i.e., zero remanence when any external magnetic field is removed).[3] For this reason, further ongoing studies are currently dedicated to extending the proposed technique to hard magnetic nanomaterials processable by AJP. This would allow the DMAJP fabrication of MSMs with more complex behavior under the action of external magnetic fields, thanks to their remanent magnetization and thus the availability of magnetic torque as well as force. Second, to further expand the process capability, different strategies for using DMAJP to fabricate truly 3D structures with more complex geometries and higher resolution are currently under investigation. Finally, further research, design studies, and development will be required depending on the specific application.

4. Experimental Section

Magnetic Ink Preparation: EMG1300M nanoparticles having polymer-coated surface modification were purchased from FerroTec Co. The particles are a 50/50 mixture of Fe_3O_4/γ-Fe_2O_3 with an average particle size of 10 nm and a weight percent of iron oxide of 60.0–80.0%. The nanoparticles were dispersed in a solution of 90% v/v toluene and 10% v/v terpineol with a concentration of 200 mg mL^{-1}. To achieve a stable colloid, sonicating, and heating of the ferrofluid at 35 °C in an ultrasound bath for 30 min was necessary.

Polymer Ink Preparation: S7,7,9-Trimethyl-4,13-dioxo-3,14-dioxa-5,12-diazahexadecane-1,16-diyl bismethacrylate (UrDMA) and 2-[[(butylamino)carbonyl]oxy]ethyl acrylate (UrA) were used as monomers. Diphenyl(2,4,6-trimethylbenzoyl)phosphine oxide (Irgacure 819) was used as photo-initiator. UrDMA/UrA mixtures (20/80 wt./wt.) containing Irgacure 819 (1.0 wt% of total monomers' mass) were prepared as photo-inks.

Printing Substrate Preparation: Glass slides were cleaned with ethanol and dried. A 5 wt% aqueous solution of poly(vinyl alcohol) (PVA, average Mw = 15 000, MP Biomedicals Europe) was deposited by spin coating (SPIN 150i, Polos) on a glass slide at 500 rpm for 120 s, forming the sacrificial layer of water-soluble polymer.

Fabrication of Polymer/Magnetic NPs/Nanocomposites: An Optomec Aerosol Jet print engine (Optomec Inc.) was engineered into a programmable 5-axis Cartesian stage controlled through a control code (G-Code) input to Aerotech A3200 Automation Controller, which moves the substrate below the aerosol to produce a pattern. The design is created in standard graphics or Computer Aided Design (CAD) software before being translated to machine control code (i.e., G-code) containing stage manipulation and DMAJP gas flow rate settings. The linear translation stages (Thorlabs DDS300/M) provide a minimum incremental movement of 100 and a 300 mm travel distance in the XY plane. The DMAJP setup is depicted as a schematic in Figure 1a. Fluoropolymer (PFA) tubes with an outer diameter of 6 mm and a wall of 1 mm were used for the connections (Swagelok). A total amount of 1.5 mL of prepared magnetic ink was placed into the glass vial designed for ultrasonicating atomization. 30 mL of the photopolymer ink was placed into a plastic jar designed for AJP for pneumatic atomization. Nitrogen was used as the inert sheath and atomizer gas. A 750 µm nozzle, a printing speed of 15 $mm^{-1}s$, a working distance of 2.5 mm, an atomizer gas flow rate, and an exhaust flow rate of the polymer aerosol respectively of 1000 SCCM and 500 SCCM were used throughout (resulting in a 500 SCMM polymer carrier gas flow rate). The carrier gas flow rate of the MNPs aerosol was varied as part of the investigation (0, 50, 60, 70, 80 SCCM). Gas flow rates are quoted in standard cubic centimeters per minute (SCCM). For the curing of the photopolymer, a UV lamp (BluWave QX4 Version 2.0 LED Spot-Curing System equipped with a 365 nm LED head and 8-mm diameter focusing lens) was integrated with the DMAJP apparatus. DMAJP deposition and UV curing are alternated in a layer-by-layer fashion until the desired number of layers is reached (Figure 1f). The required curing time for each layer is 3 s with a final post-curing of 60 s. After the curing, the immersion of the sample in a petri dish filled with deionized water allows the dissolution of the sacrificial layer and the subsequent release of the printed structure.

Morphological Characterization of the Printed Composite Structures: For a preliminary investigation of the DMAJP printed nanocomposite films, optical images were taken by Olympus-BX53 microscope (Olympus), covering a magnification range from 2.5× to 50×. Scanning electron microscopy and Energy Dispersive X-ray (EDX) analysis of the samples were performed with a GeminiSEM 300 scanning electron microscope (Zeiss). The samples were glued onto the conductive base and sputtered with a platinum layer (thickness 4 nm) to avoid electrical charges. The SEM images were taken at an accelerating voltage of 5 kV. The EDX investigations were carried out at a higher accelerating voltage (15 kV). Thickness measurements were performed using a white confocal light microscope (NPFLEX-1000, Bruker).

Thermogravimetric Analysis: Thermogravimetric analysis (TGA) of the DMAJP printed nanocomposite films was done using a Thermal Analysis System TGA 2 (Mettler Toledo). TGA experiments were performed on samples of ≈10 mg from 20 up to 600 °C at a heating rate of 10 °C min^{-1} under nitrogen atmospheres, with a gas purge rate of 50 mL min^{-1}.

Magnetic Characterization: The remanent magnetization and memory effect measurements under FC-ZFC protocols of the DMAJP printed nanocomposite films were investigated using a superconducting quantum interference measurement device – vibrating sample magnetometer (SQUID-VSM from Quantum Design). The magnetization curves were recorded for pristine EMG1300M nanoparticles and for MNP-CF_x samples. The hysteresis loops were measured at 300 K by cyclically applying a magnetic field up to ±20 kOe.

Supporting Information

Supporting Information is available from the Wiley Online Library or from the author.

Acknowledgements

This work is funded by the UK Engineering and Physical Sciences Research Council (EPSRC) under grant EP/V009818/1 and EP/P027687/1.

Conflict of Interest

The authors declare no conflict of interest.

Data Availability Statement

The data that support the findings of this study are available from the corresponding author upon reasonable request.

Keywords

aerosol jet printing, digital manufacturing, magnetic polymer composites, multi-material printing, soft robotics, tailorable composites

Received: March 21, 2024
Revised: June 12, 2024
Published online: June 22, 2024

[1] a) H. Cui, Q. Zhao, Y. Wang, X. Du, *Chemistry – An Asian Journal* **2019**, *14*, 2369; b) J. Kim, J. W. Kim, H. C. Kim, L. Zhai, H.-U. Ko, R. M. Muthoka, *International Journal of Precision Engineering and Manufacturing* **2019**, *20*, 2221; c) M. Wei, Y. Gao, X. Li, M. J. Serpe, *Polym. Chem.* **2017**, *8*, 127; d) Q. Zheng, C. Xu, Z. Jiang, M. Zhu, C. Chen, F. Fu, *Frontiers in Chemistry* **2021**, *9*, 650358.

[2] a) A. K. Bajpai, S. K. Shukla, S. Bhanu, S. Kankane, *Prog. Polym. Sci.* **2008**, *33*, 1088; b) C. De las Heras Alarcón, S. Pennadam, C. Alexander, *Chem. Soc. Rev.* **2005**, *34*, 276; c) L. Hines, K. Petersen, G. Z. Lum, M. Sitti, *Adv. Mater.* **2017**, *29*, 1603483; d) A. Kirillova, L. Ionov, *J. Mater. Chem. B* **2019**, *7*, 1597; e) Z. Shen, F. Chen, X. Zhu, K.-T. Yong, G. Gu, *J. Mater. Chem. B* **2020**, *8*, 8972; f) A. Zhang, K. Jung, A. Li, J. Liu, C. Boyer, *Prog. Polym. Sci.* **2019**, *99*, 101164.

[3] Y. Kim, X. Zhao, *Chem. Rev.* **2022**, *122*, 5317.

[4] a) A. K. Bastola, M. Hossain, *Mater. Des.* **2021**, *211*, 110172; b) N. Bira, P. Dhagat, J. R. Davidson, *Frontiers in Robotics and AI* **2020**, *7*, 588391; c) H. J. Chung, A. M. Parsons, L. Zheng, *Advanced Intelligent Systems* **2021**, *3*, 2000186; d) N. Ebrahimi, C. Bi, D. J. Cappelleri, G. Ciuti, A. T. Conn, D. Faivre, N. Habibi, A. Hošovský, V. Iacovacci, I. S. Khalil, *Adv. Funct. Mater.* **2021**, *31*, 2005137; e) S. Wu, W. Hu, Q. Ze, M. Sitti, R. Zhao, *Multifunctional materials* **2020**, *3*, 042003.

[5] a) M. Eshaghi, M. Ghasemi, K. Khorshidi, *Extreme Mechanics Letters* **2021**, *44*, 101268; b) Y. Kim, G. A. Parada, S. Liu, X. Zhao, *Sci. Rob.* **2019**, *4*, eaax7329; c) P. Lloyd, A. K. Hoshiar, T. da Veiga, A. Attanasio, N. Marahrens, J. H. Chandler, P. Valdastri, *IEEE Robotics and Automation Letters* **2020**, *5*, 3937; d) G. Pittiglio, J. H. Chandler, T. da Veiga, Z. Koszowska, M. Brockdorff, P. Lloyd, K. L. Barry, R. A. Harris, J. McLaughlan, C. Pompili, *Communications Engineering* **2023**, *2*, 50; e) S. Yim, M. Sitti, *IEEE Transactions on Robotics* **2011**, *28*, 183; f) M. H. D. Ansari, V. Iacovacci, S. Pane, M. Ourak, G. Borghesan, I. Tamadon, E. Vander Poorten, A. Menciassi, *Adv. Funct. Mater.* **2023**, *33*, 2211918; g) Y. Dong, L. Wang, N. Xia, Z. Yang, C. Zhang, C. Pan, D. Jin, J. Zhang, C. Majidi, L. Zhang, *Sci. Adv.* **2022**, *8*, eabn8932.

[6] a) Z. Ji, C. Yan, B. Yu, X. Wang, F. Zhou, *Adv. Mater. Interfaces* **2017**, *4*, 1700629; b) E. B. Joyee, Y. Pan, *J. Manuf. Processes* **2020**, *56*, 1178; c) J. Zhang, Z. Ren, W. Hu, R. H. Soon, I. C. Yasa, Z. Liu, M. Sitti, *Sci. Rob.* **2021**, *6*, eabf0112.

[7] a) Z. Ren, W. Hu, X. Dong, M. Sitti, *Nat. Commun.* **2019**, *10*, 2703; b) V. K. Venkiteswaran, L. F. P. Samaniego, J. Sikorski, S. Misra, *IEEE Robotics and Automation Letters* **2019**, *4*, 1753; c) C. Wang, V. R. Puranam, S. Misra, V. K. Venkiteswaran, *IEEE Robotics and Automation Letters* **2022**, *7*, 5795; d) Y. Deng, Y. Zhao, J. Zhang, T. Arai, Q. Huang, X. Liu, *Advanced Intelligent Systems* **2024**, *6*, 2300471.

[8] A. Bandyopadhyay, B. Heer, *Mater. Sci. Eng.: R: Rep.* **2018**, *129*, 1.
[9] D. Han, H. Lee, *Curr. Opin. Chem. Eng.* **2020**, *28*, 158.
[10] a) D. Jang, D. Kim, J. Moon, *Langmuir* **2009**, *25*, 2629; b) Y. Guo, H. S. Patanwala, B. Bognet, A. W. Ma, *Rapid Prototyping J.* **2017**, *23*, 562; c) Y. L. Tee, C. Peng, P. Pille, M. Leary, P. Tran, *Jom* **2020**, *72*, 1105.
[11] J. Simińska-Stanny, M. Nizioł, P. Szymczyk-Ziółkowska, M. Brożyna, A. Junka, A. Shavandi, D. Podstawczyk, *Addit. Manuf.* **2022**, *49*, 102506.
[12] E. B. Joyee, A. Szmelter, D. Eddington, Y. Pan, *Soft Robotics* **2022**, *9*, 1.
[13] a) S. Hasanov, S. Alkunte, M. Rajeshirke, A. Gupta, O. Huseynov, I. Fidan, F. Alifui-Segbaya, A. Rennie, *J. Manuf. Mater. Process.* **2021**, *6*, 4; b) J.-W. Choi, H.-C. Kim, R. Wicker, *J. Mater. Process. Technol.* **2011**, *211*, 318.
[14] M. Y. Khalid, Z. U. Arif, A. Tariq, M. Hossain, K. A. Khan, R. Umer, *Eur. Polym. J.* **2024**, *205*, 112718.
[15] N. Wilkinson, M. Smith, R. Kay, R. Harris, *JAMT* **2019**, *105*, 4599.
[16] T. Seifert, E. Sowade, F. Roscher, M. Wiemer, T. Gessner, R. R. Baumann, *Ind. Eng. Chem. Res.* **2015**, *54*, 769.
[17] a) C. Areias, Y. Piro, O. Ranasingha, A. Akyurtlu, *Flex. Print. Electron.* **2023**, *8*, 015009; b) M. Seiti, O. Degryse, E. Ferraris, *Mater. Today: Proc.* **2022**, *70*, 38.
[18] a) K. Wang, Y.-H. Chang, C. Zhang, B. Wang, *Carbon* **2016**, *98*, 397; b) M. Zeng, Y. Du, Q. Jiang, N. Kempf, C. Wei, M. V. Bimrose, A. N. M. Tanvir, H. Xu, J. Chen, D. J. Kirsch, J. Martin, B. C. Wyatt, T. Hayashi, M. Saeidi-Javash, H. Sakaue, B. Anasori, L. Jin, M. D. McMurtrey, Y. Zhang, *Nature* **2023**, *617*, 292.
[19] a) Q. Jing, Y. S. Choi, M. Smith, C. Ou, T. Busolo, S. Kar-Narayan, *Adv. Mater. Technol.* **2019**, *4*, 1900048; b) C. Ou, A. L. Sangle, T. Chalklen, Q. Jing, V. Narayan, S. Kar-Narayan, *APL Mater.* **2018**, 6.
[20] C. Ou, A. L. Sangle, A. Datta, Q. Jing, T. Busolo, T. Chalklen, V. Narayan, S. Kar-Narayan, *ACS Appl. Mater. Interfaces* **2018**, *10*, 19580.
[21] M. T. Craton, J. D. Albrecht, P. Chahal, J. Papapolymerou, *IEEE Trans. Compon., Packag., Manuf. Technol.* **2021**, *11*, 865.
[22] S. Taccola, T. da Veiga, J. H. Chandler, O. Cespedes, P. Valdastri, R. A. Harris, *Sci. Rep.* **2022**, *12*, 17931.
[23] a) H. Bakhshi, G. Kuang, F. Wieland, W. Meyer, *Polymers* **2022**, 14; b) N. Singh, H. Bakhshi, W. Meyer, *RSC Adv.* **2020**, *10*, 44103.
[24] a) R. Jahn, T. Jung, *Prog. Org. Coat.* **2001**, *43*, 50; b) C. Mendes-Felipe, A. Garcia, D. Salazar, J. Vilas-Vilela, S. Lanceros-Mendez, *Composites Part C: Open Access* **2021**, *5*, 100143; c) T. Nardi, M. Sangermano, Y. Leterrier, P. Allia, P. Tiberto, J.-A. E. Månson, *Polymer* **2013**, *54*, 4472.
[25] A. Ditsch, P. E. Laibinis, D. I. Wang, T. A. Hatton, *Langmuir* **2005**, *21*, 6006.
[26] C. de Montferrand, L. Hu, I. Milosevic, V. Russier, D. Bonnin, L. Motte, A. Brioude, Y. Lalatonne, *Acta Biomater.* **2013**, *9*, 6150.
[27] S. Taccola, A. Desii, V. Pensabene, T. Fujie, A. Saito, S. Takeoka, P. Dario, A. Menciassi, V. Mattoli, *Langmuir* **2011**, *27*, 5589.
[28] Á. Díaz-García, J. Y. Law, M. Felix, A. Guerrero, V. Franco, *Mater. Des.* **2022**, *219*, 110806.